POLYOXOMETALATES

Open Access
RESEARCH ARTICLE

Engineering boron-imidazolate-based polyoxometalates for photooxidative C=C bond cleavage in aqueous media

Jiajia Wang[1], Zhaoyang Wu[1], Qun Li[1], Hanlei Zhang[1], Yang Liu[1], Guixiao Ji[1], Yalin Zhang[1] ✉, Qianli Li[1], Junyu Ren[3] ✉, Qingde Zhang[2], and Xianqiang Huang[1] ✉

[1] *Shandong Provincial Key Laboratory of Chemical Energy Storage and Novel Cell Technology, School of Chemistry & Chemical Engineering, Liaocheng University, Liaocheng 252059, China*
[2] *State Key Laboratory of Coal Conversion, Institute of Coal Chemistry, Chinese Academy of Sciences, Taiyuan 030001, China*
[3] *Department of Chemical and Biomolecular Engineering, National University of Singapore, 4 Engineering Drive 4, Singapore 117585, Singapore*

Cite This: *Polyoxometalates*, **2025**, *4*, 9140087

Read Online

ABSTRACT: The direct cleavage of alkenes to access value-added carbonyls under solar-driven conditions in aqueous media presents a considerable challenge. Addressing this challenge requires the construction of effective visible-light-responsive catalysts. Herein, two boron-imidazolate-based Strandberg-type polyoxomolybdophosphate hybrids, $Co(H_2O)_4[HP_2Mo_5O_{23}]_2[B(HIM)(IM)_2]_2[B(HIM)_3]_2 \cdot 12H_2O$ (**1**) and $Zn(H_2O)_4[HP_2Mo_5O_{23}]_2[B(HIM)(H_2IM)_2]_4 \cdot 7H_2O$ (**2**) (IM = imidazole), were synthesized using a hydrothermal method and were utilized as efficient photocatalysts for the aerobic oxidative C=C bond cleavage of alkenes under natural sunlight and aqueous phase conditions. The incorporation of boron imidazolate ligands broadened the visible-light absorption region of polyoxometalates, and electrochemical tests highlighted their potential as exceptional photocatalysts. Upon visible blue light irradiation and ambient O_2 pressure in aqueous media, compound **1** exhibited remarkable aerobic photocatalytic activity, efficiently cleaving alkenes to yield the corresponding ketones (yields up to 91%). Notably, its catalytic performance remained consistent after three recycling runs under ambient sunlight, highlighting its robust stability and practical applicability. Subsequent mechanistic investigations revealed the involvement of $O_2^{\cdot-}$ species in the reaction, and a possible mechanism for the cleavage of the alkenes was proposed.

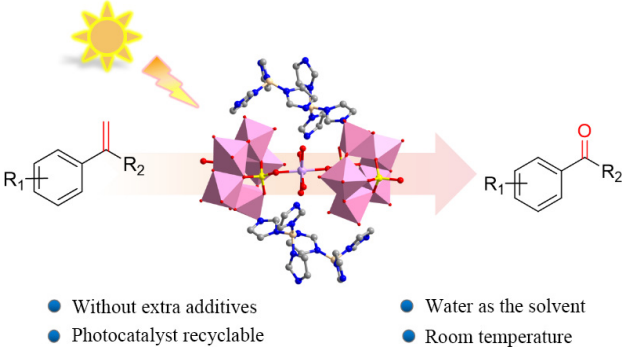

KEYWORDS: boron imidazolate, polyoxometalates, photooxidative cleavage, alkenes

1 Introduction

The selective aerobic oxidative cleavage of commercially available alkenes to access value-added ketones is one of the most fundamental organic transformations in organic synthesis [1–3]. Traditional protocols involve the use of high-valence metals and stoichiometric oxidants [4–6]. However, these techniques have encountered challenges related to high costs, hazardous materials, the generation of toxic waste oxidants, and cumbersome handling procedures. Consequently, the application of greener oxidants such as molecular oxygen in the synthesis of aldehydes and ketones has garnered significant interest, particularly in light of the demand for sustainable processing and the utilization of abundant feedstocks. For example, Jiao et al. developed a process catalyzed by *N*-hydroxyphthalimide to convert aromatic alkenes into ketones in the presence of molecular oxygen [7]. Xiao et al. described an approach for selective cleavage using an iron catalyst in conjunction with an unconventional bisimidazoline ligand in an oxygen atmosphere [8].

Meanwhile, visible light is abundant and readily available, offering great potential for facilitating environmentally friendly chemical reactions. Therefore, the development of sustainable photochemical methods to synthesize carbonyl compounds using molecular oxygen has become a critical pursuit. In this regard, Xiao et al. achieved the aerobic cleavage of aromatic and aliphatic alkenes with a $[Mn(dtbpy)_2(OTf)_2]$ (dtbpy = 4,4'-ditert-butyl-2,2'-dipyridine, Otf = trifluoromethanesulfonate) as a photocatalyst [9]. In 2021, Du et al. used $Bu_4N[W_{10}O_{32}]$ as a photosensitizer and 18-crown-6 as an additive and realized the oxidative cleavage of the olefin double bond in an aqueous solvent [10]. Recently, Li et al. developed an imidazole-linked porphyrin-based covalent organic framework with red light absorption that served as a

Received: December 4, 2024; **Revised:** February 3, 2025
Accepted: February 16, 2025

✉Address correspondence to Yalin Zhang, zhangyalin@lcu.edu.cn; Junyu Ren, junyuren@nus.edu.sg; Xianqiang Huang, hxqqxh2008@163.com

https://doi.org/10.26599/POM.2025.9140087

photosensitizer for catalyzing the oxidative cleavage of alkenes [11]. However, although the above photocatalysts have been effective in organic transformations, their complex preparation and need for additional additives have limited their broader use. Therefore, there is an urgent need to identify effective photocatalytic systems that respond to visible light and enable the oxidative cleavage of alkenes in a mild and environmentally friendly manner.

Polyoxometalates (POMs), a large class of transition metal–oxide clusters with excellent redox-active and reversible electron-transfer properties [12, 13], have exhibited significant and wide-ranging applications in catalysis [14–28], medicine [29], energy storage [30], and organic transformation [31]. Nevertheless, most bulk POMs exhibit limited adsorption of visible light and often encounter challenges such as low surface area and poor light-harvesting capacity [32, 33], which inevitably restrict the practical utilization of POM-based photocatalysts. To address these issues, several strategies have been developed to integrate POMs with supports, forming POM-based hybrid materials that extend their absorption into the visible region [34–40]. In addition, boron imidazolates have been explored as promising organic ligands in coordination chemistry given their unique advantages, including zeolitic topologies and controllable tetrahedral and tripodal coordination modes [41–43]. However, boron imidazolate-based POMs are very rare, as confirmed by a Cambridge Structural Database search, as is their use in combination with visible light to drive the photooxidative cleavage of alkenes in aqueous media.

Herein, two boron imidazolate-based POM hybrids, $Co(H_2O)_4[HP_2Mo_5O_{23}]_2[B(HIM)(IM)_2]_2[B(HIM)_3]_2 \cdot 12H_2O$ (**1**) and $Zn(H_2O)_4[HP_2Mo_5O_{23}]_2[B(HIM)(H_2IM)_2]_4 \cdot 7H_2O$ (**2**) (IM = imidazole), were synthesized successfully. Structural analysis reveals that the frameworks are composed of transition metal cations ($[Co(H_2O)_4]^{2+}$ and $[Zn(H_2O)_4]^{2+}$), polyoxoanions, and boron imidazolate cations (Fig. 1). Compound **1** represents the first crystal structure constructed from boron imidazolate and POMs. The photocatalytic efficiency for C=C bond cleavage to produce ketones was assessed at room temperature under 400–405 nm of LED (10 W) irradiation, with O_2 serving as the oxidant. The catalysts demonstrate excellent activity and good recyclability for the oxidative cleavage of alkenes into ketones. This mechanism underscores the indispensable role of superoxide radicals in driving reaction processes. This work elucidates the strategic design and synthesis of white-light-responsive POMs, highlighting their potential as efficient and sustainable photocatalysts for industrial transformations.

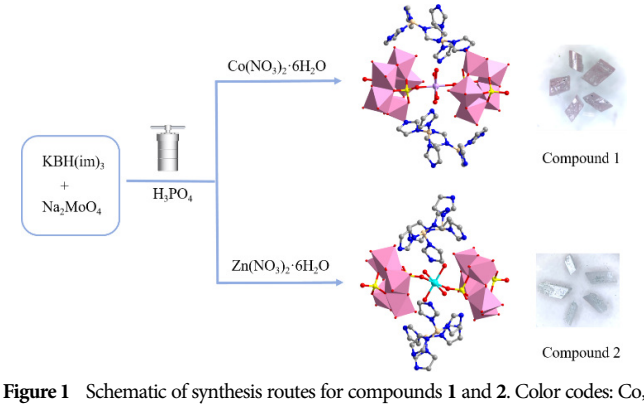

Figure 1 Schematic of synthesis routes for compounds **1** and **2**. Color codes: Co, purple; Zn, turquoise; Mo, pink; P, brilliant yellow; B, light yellow; N, blue; O, red; C, gray.

2 Experimental

2.1 Synthesis of compound 1

$Na_2MoO_4 \cdot 2H_2O$ (0.24 g, 0.1 mmol), $Co(NO_3)_2 \cdot 6H_2O$ (0.07 g, 0.25 mmol), and $KBH(IM)_3$ (0.050 g, 0.2 mmol) were sealed in a 25-mL Teflon-lined autoclave in the CH_3OH/H_2O (2 mL/10 mL), and the pH of the mixture was adjusted to 2.00 by adding 3-M H_3PO_4. The mixture was heated at 90 °C for 120 h and then cooled slowly to room temperature. The pink block crystals of compound **1** were obtained and washed three times with distilled water and air-dried. Yield: 86%. Anal. Calcd. for $C_{36}H_{74}N_{24}O_{60}P_4CoMo_{10}B_4$: C, 14.47; H, 2.50; N, 11.25; Co, 1.97; Mo, 32.10. Found: C, 14.42; H, 2.51; N, 11.34; Co, 1.89; Mo, 32.17. Fourier transform infrared (FT-IR) spectrum (KBr pellet, cm^{-1}): 3454 (s, O–H), 3129 (m, N–H), 1562 (m, C=N), 1447 (m, C–C), 1337 (m, C–N), 1237 (s, B–N), 1089 (s, P–O), 917 (s, Mo–O_t), 668 (s, O_b–Mo–O_b).

2.2 Synthesis of compound 2

The synthesis of compound **2** was similar to that of compound **1**, except that $Zn(NO_3)_2 \cdot 3H_2O$ was used instead of $Co(NO_3)_2 \cdot 6H_2O$ and the pH value of the resulting solution was adjusted to 3.00. The resulting colorless block crystals were collected and dried. Yield: 62%. Anal. Calcd. for $C_{36}H_{80}N_{24}O_{63}P_4Mo_{10}ZnB_4$: C, 14.18; H, 2.64; N, 11.03; Zn, 2.14; Mo, 31.47. Found: C, 14.05; H, 2.72; N, 11.34; Zn, 2.18; Mo, 35.17. FT-IR spectrum (KBr pellet, cm^{-1}): 3477 (s, O–H), 3134 (m, N–H), 1576 (m, C=N), 1452 (m, C–C), 1337 (m, C–N), 1237 (m, B–N), 1089 (m, P–O), 917 (s, Mo–O_t), 668 (s, O_b–Mo–O_b).

2.3 General procedure for photooxidative alkene cleavage

Alkenes (0.2 mmol), compound **1** (30 mg, 5 mol%), and H_2O (0.5 mL) were placed in an oven-dried quartz tube with a magnetic stir bar. The mixture was irradiated for 24 h with blue LEDs (10 W, 400–405 nm) under a 1-atm oxygen atmosphere at 25 °C. After the reaction was completed, the resulting solution was analyzed using proton nuclear magnetic resonance (^1H NMR) and gas chromatography–mass spectrometry analysis.

3 Results and discussion

3.1 Structure description

Single X-ray crystal diffraction analyses indicate that compounds **1** and **2** both crystallized in the triclinic space system with the $P\bar{1}$ space group (Table S1 in the Electronic Supplementary Material (ESM)) and consisted of similar $\{P_2Mo_5\}$ units: the Co/Zn cations and the protonated boron imidazolate cations. As compounds **1** and **2** are isostructural, only the crystal structure of compound **1** is described in detail as a representative view here.

As shown in Figs. 1 and 2, the crystals of compound **1** contain one $[Co(H_2O)_4]^{2+}$ cation, two $[P_2Mo_5O_{23}]^{6-}$ polyanions, four protonated boron imidazolate cations, and 12 lattice water molecules. The Co1 atom of the $[Co(H_2O)_4]^{2+}$ cation is six-coordinated by two O3 atoms from the capped PO_4 tetrahedron and four oxygen atoms (O1, O2) from the coordinated water molecules and adopts a distorted octahedron geometry. For the polyoxoanions, the P_2Mo_5 cluster comprises five distorted MoO_6 octahedra along with two capped PO_4 tetrahedra on either side. The presence of H^+ ions in the acidic environment induces the cleavage

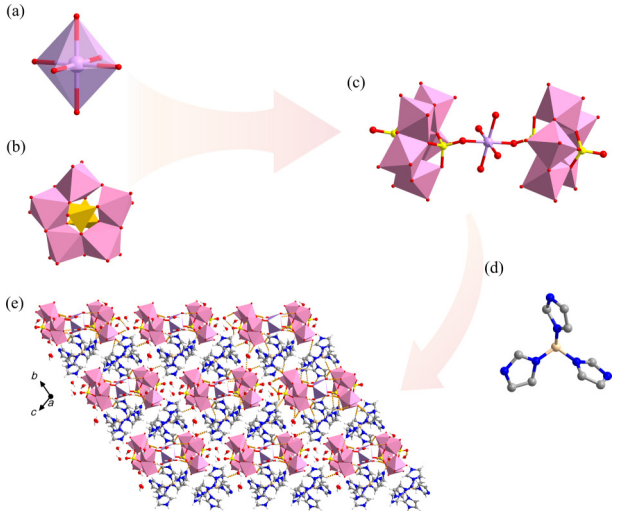

Figure 2 (a) The coordination mode of Co atom in compound **1**; (b) structure of the Strandberg anion; (c) structural representation for $Co(H_2O)_4[HP_2Mo_5O_{23}]_2^{8-}$; (d) structure of boron imidazolate; (e) 3D supramolecular framework of compound **1**.

of the B–H bond in the boron imidazole ligand, leading to the removal of the hydride from the boron atom. Simultaneously, some nitrogen atoms in the imidazole ring are protonated, resulting in the formation of the boron imidazole cation. The $[Co(H_2O)_4]^{2+}$ cation and two $[P_2Mo_5O_{23}]^{6-}$ polyanions are bridged by Co–O bonds and achieve the $Co(H_2O)_4[HP_2Mo_5O_{23}]_2^{8-}$ unit, which is further linked by strong hydrogen bond interactions with the boron imidazolate cations to form a stable three-dimensional (3D) framework (Fig. 2(e)). Similarly, compound **2** can also form an analogous 3D framework (Fig. S1 in the ESM). The bond lengths of the Co–O, P–O, and Mo–O bonds range from 2.063(14) to 2.111(13) Å, 1.509(14) to 1.72(2) Å, and 1.661(17) to 2.363(14) Å, respectively. Bond valence sum calculations reveal that the oxidation state values of Co and Mo in compound **1** are +2 and +6, respectively (Table S6 in the ESM), which is in excellent agreement with the X-ray photoelectron spectroscopy (XPS) results.

3.2 Characterization of compounds 1 and 2

To further verify the structural characteristics of the boron imidazolate-based POMs, compounds **1** and **2** were characterized using FT-IR spectroscopy, powder X-ray diffraction (PXRD), and thermogravimetric analysis (TGA). As shown in Fig. S2 in the ESM, their similar FT-IR spectra indicate the presence of analogous components and functional groups. Our analysis focused on compound **1** as an example. The absorption bands at 3454 and 3129 cm^{-1} for compound **1** can be attributed to the stretching vibrations of the O–H and N–H bonds, respectively. The characteristic peak at 1562 cm^{-1} is attributed to C=N vibrations. The absorption peaks at 1447–1337 cm^{-1} are assigned to the stretching vibrations of the C–C and C–N bonds in the boron imidazole ligand. The strong band at 1237 cm^{-1} is related to B–N bonds. Additionally, all compounds display characteristic absorption bands associated with the $\{P_2Mo_5\}$ POM anion: The bands in the range of 1012–1132 cm^{-1} are attributed to P–O vibrations; the peaks at 917 cm^{-1} correspond to the Mo–O_t stretching vibrations (O_t: terminal oxygen atom); and the peak at 668 cm^{-1} is assigned to the O_b–Mo–O_b stretching vibrations (O_b: bridging oxygen atom).

The PXRD patterns of the as-synthesized compounds **1** and **2** are in accordance with the simulated patterns (Fig. S3 in the ESM), confirming the high purity of the obtained samples. Meanwhile, the chemical stability of the boron-imidazolate-based POM **1** was examined after treating it using various solvents (dimethyl carbonate, H_2O, methanol, tetrahydrofuran (THF), dimethylformamide, and ethanol) and aqueous acidic and basic solutions (across a pH range of 1–12) for 24 h at room temperature (Fig. 3). The PXRD patterns retained their structural integrity after 24 h with a pH range of 1–9, suggesting good stability with no phase transition (Fig. 3(a)), whereas notable differences in the PXRD patterns of compound **1** emerged when the pH reaches 12. In addition, the prepared compound **1** maintained its crystallinity in different polar solvents (Fig. 3(b)), indicating its strong structural stability.

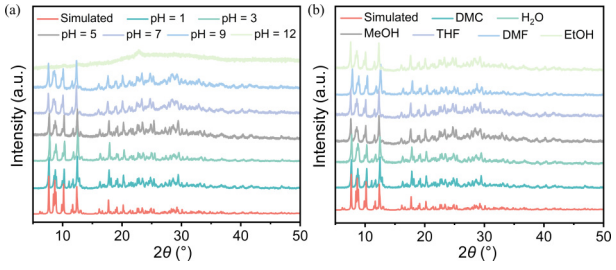

Figure 3 PXRD patterns of compound **1** after immersed in (a) aqueous solutions with pH range of 1–12 and (b) various solvents.

The thermal stabilities of compounds **1** and **2** were studied using TGA (Fig. S4 in the ESM). The TGA results for compound **1** showed that two steps of weight loss occurred in the range of 30–800 °C. The initial weight loss of 7.8% (calc. 7.2%) occurred between 30 and 162 °C, which was due to the loss of crystal water molecules. The second case in the range of 245 to 550 °C might have been caused by the thermal decomposition of the coordinated water molecules, boron imidazolate ligand, and polyoxoanion skeletons. Similarly, compound **2** exhibited a two-step weight loss from 30–800 °C. The first loss, 5.1% (calcd. 4.1%), occurred between 30 and 96 °C and was attributed to crystal water loss. Following this process, the coordination of water molecules, boron imidazolate ligands, and polyoxoanion skeletons occurred between 275 and 570 °C.

3.3 Photocatalytic properties

The optical properties of a photocatalyst are the key factors that influence the efficiency of photocatalysis. Ultraviolet–visible (UV–vis) diffuse reflectivity spectroscopy (DRS) was used to investigate the light absorption of the studied photocatalysts. As depicted in Fig. 4(a), the light absorption of compound **1** was mainly in the range of 200–580 nm, whereas that of compound **2** was primarily in the range of 200–460 nm. Furthermore, band-gap energies (E_g) of 3.03 eV for compound **1** and 3.13 eV for compound **2** were obtained using the Kubelka–Munk equation, which indicated their semiconductor-like characteristics (Fig. 4(b)). In addition, Mott–Schottky measurements were performed at the frequencies of 1000, 2000, and 3000 Hz (Figs. 4(c) and 4(d)). The flat-band potentials measured for compounds **1** and **2** were −0.72 and −0.76 V (vs. Ag/AgCl), respectively. The conduction band lowest unoccupied molecular orbital (LUMO) energy values for compounds **1** and **2** determined as −0.52 V vs. normal hydrogen electrode (NHE) and −0.56 V vs. NHE indicated that both compounds can thermodynamically complete the O_2 activation

process ($E(O_2/O_2^{\bullet-})$ = −0.33 V vs. NHE). The highest occupied molecular orbital energy levels were further calculated from the E_g and LUMO of compounds **1** and **2** as 2.51 V (vs. NHE) and 2.57 V (vs. NHE), respectively. In addition, the electrochemical impedance spectroscopy and transient photocurrent intensity of compounds **1** and **2** under visible-light irradiation were further evaluated to explore their specific photovoltaic properties. The electrochemical impedance spectrum (Fig. 4(e)) shows that compound **1** had a smaller semicircle size than compound **2**, indicating a higher photogenerated electron-transfer efficiency for compound **1**. As shown in Fig. 4(f), both compounds **1** and **2** exhibited distinct transient photocurrent responses over eight consecutive on–off irradiation cycles, indicating a low recombination efficiency of the photogenerated electron–hole pairs. Furthermore, compound **1** showed a significantly higher photocurrent than compound **2**, suggesting that compound **1** is more effective in photogenerated charge separation and transfer.

3.4 Photocatalytic oxidative cleavage of aromatic alkenes

To assess the photocatalytic efficacy of the as-obtained catalysts, the oxidative cleavage of aromatic alkenes to ketones was employed as a model reaction. Specifically, 1,1-diphenylethylene (**1a**) was selected as the model substrate for this evaluation. Initially, we performed the reaction with 20 mg (3.3 mol%) of the catalyst (compounds **1** and **2**) in 0.5-mL H_2O at 1-atm O_2 under blue LED light for 24 h. Compound **1** was superior to compound **2** with good efficiency, generating **1b** in 87% yield. We speculated that this outcome may be attributed to the influence of cobalt having a $3d^7$ electron configuration on the coordination field via d–d transitions, which enhanced the light absorption capacity of compound **1**. Using a catalyst composed of $Co(NO_3)_2$ and $KBH(IM)_3$ ligands in a molar ratio of 1:4, the yield of diphenyl ketone **1b** was 64%. In contrast, the yield was 50% when $P_2Mo_5((NH_4)_6[P_2Mo_5O_{23}])$ was used as the catalyst. When a catalyst mixture of P_2Mo_5, $Co(NO_3)_2$, and $KBH(IM)_3$ ligands was employed, the yield was 70% (Fig. 5(a)). Subsequently, different light sources, such as red, green, and white LEDs, were tested in sequence, with blue light yielding the best results. When the reaction was performed in the dark, no desired product was detected (Fig. 5(b)). The use of other solvents, including MeCN, dioxane, DMA, and THF, was found to be less

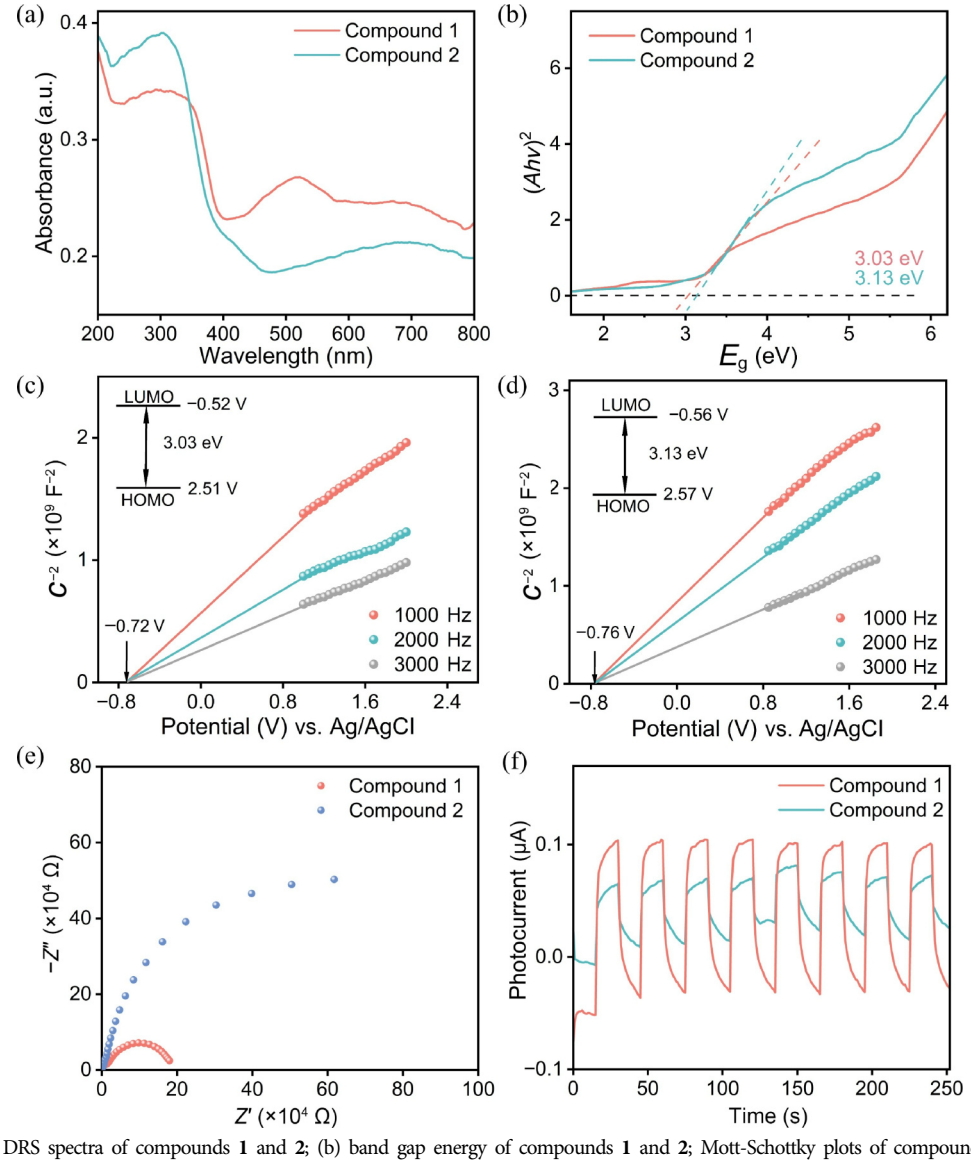

Figure 4 (a) UV–vis DRS spectra of compounds **1** and **2**; (b) band gap energy of compounds **1** and **2**; Mott-Schottky plots of compounds **1** (c) and **2** (d); (e) electrochemical impedance spectra of compounds **1** and **2**; (f) transient photocurrent curves of compounds **1** and **2**.

efficient (Fig. 5(c)). Additionally, we screened the loading of compound **1**, and the yield increased to 91% with the use of 30 mg (5 mol%) of compound **1**, and the excessive catalyst notably decreased the yield because of the generation of overoxidated products (Fig. 5(d)). Thereafter, the effect of the light source power on the yield was examined, and the yield was the highest when the wattage reached 10 W (Fig. 5(e)). Finally, using compound **1** as the catalyst and H_2O as the solvent for time screening, a 91% yield of **1b** was achieved after 24 h (Fig. 5(f)).

Under the optimized conditions, we proceeded to examine various 1,1-diphenylethylene derivatives substituted with electron-donating groups (Me) or electron-withdrawing groups (Cl, F) (Table 1). The corresponding ketones were obtained in good yields (81%–85%). Monosubstituted compounds bearing CH_3 or Cl (entries 5 and 6) substituents were suitable, affording the desired products in 84% or 81% yields, respectively. The results indicated that the electronic effectsof the substituents have a minor impact on the catalytic efficiency. In addition, this protocol is also tolerant for a-methyl styrene, as acetophenone and its CH_3 or Cl substituted derivatives were generated with moderate yields (entries 7–9). Significantly, dialene can feasibly form the desired dicarbonyl compound with oxidative cleavage of the double C=C bonds (entry 10).

Moreover, the separability and recyclability of the catalyst played crucial roles in the designed catalytic system. The reusability and heterogeneity of compound **1** were evaluated using the photocatalytic reaction of the oxidative cleavage of **1a** to benzophenone as the model. After three cycles, the catalyst was easily separated from the reaction mixture by centrifugation. Notably, no significant drop in yield was observed (first run, 91%;

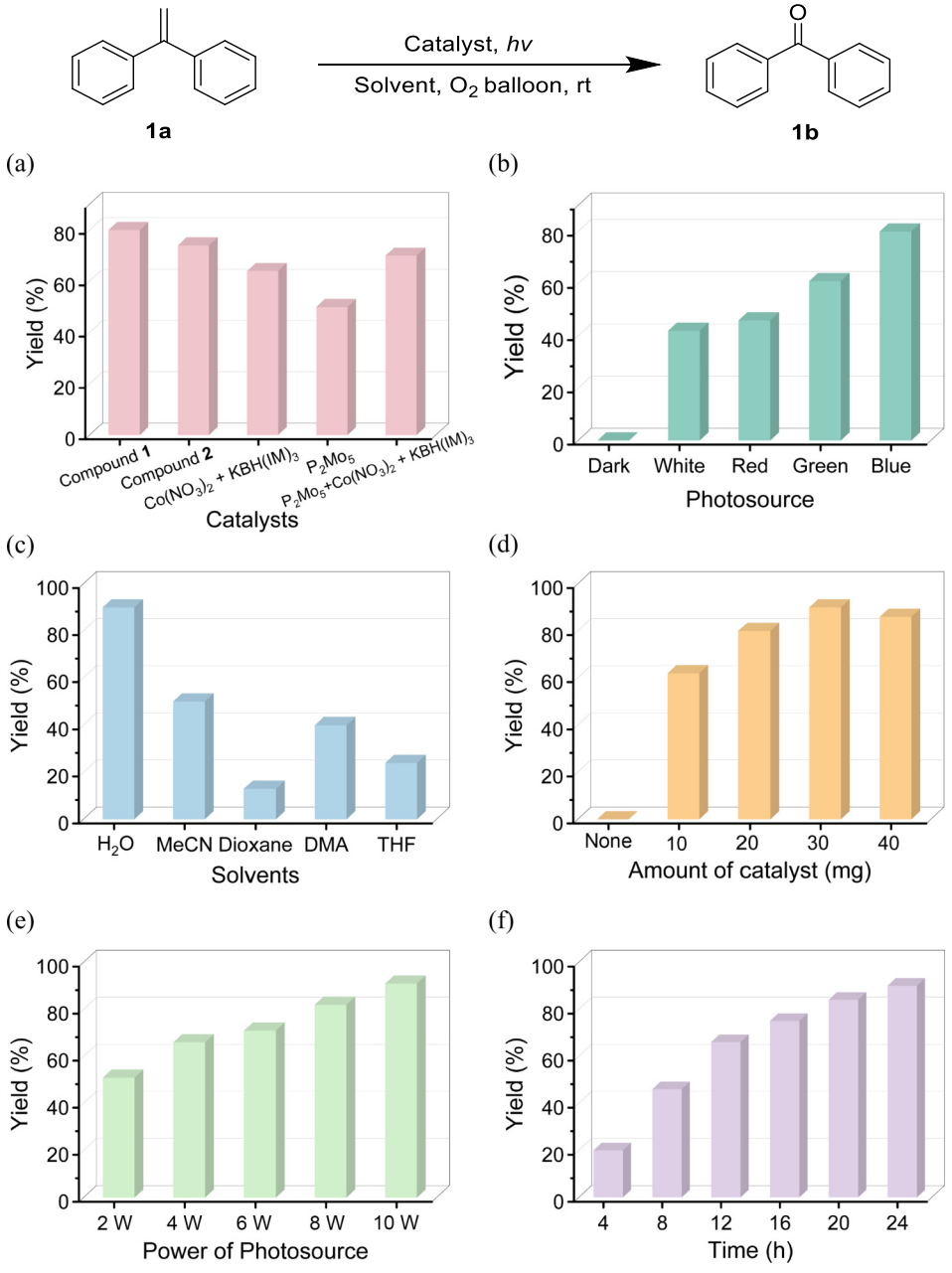

Figure 5 (a) Influence of different catalysts; (b) light source effect; (c) solvent effect; (d) catalyst amount effect; (e) effect of photosource power; (f) reaction time profile. Reaction conditions: **1a** (0.2 mmol), O_2 balloon, catalyst and 0.5 mL solvents, 25 °C.

Table 1 Scope of oxidative cleavage of aromatic alkenes[a]

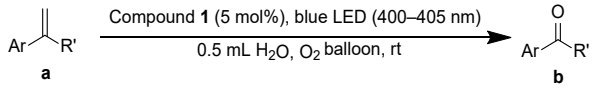

Entry	Substrates	Products	Yield (%)[b]
1	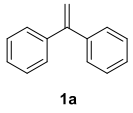 1a	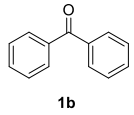 1b	91
2	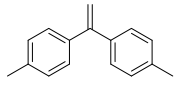 2a	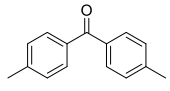 2b	85
3	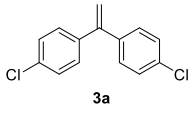 3a	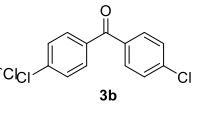 3b	81[c]
4	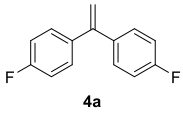 4a	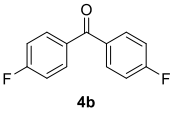 4b	82
5	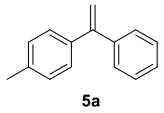 5a	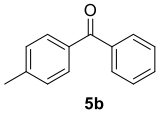 5b	84
6	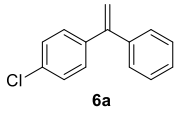 6a	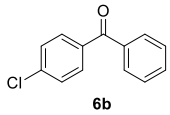 6b	81
7	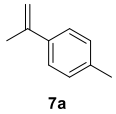 7a	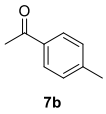 7b	66
8	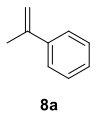 8a	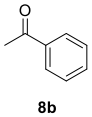 8b	64
9	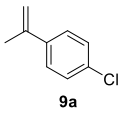 9a	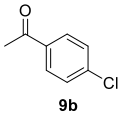 9b	63
10	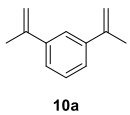 10a	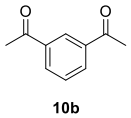 10b	57

[a] **1a** (0.2 mmol), compound **1** (5 mol%), H_2O (0.5 mL), O_2 balloon, at 25 °C, blue LED (400–405 nm, 10 W) for 24 h. [b] Yields were determined by ^1H NMR calibration using CH_2Br_2 as internal standard. [c] MeCN:H_2O (1:1, 1 mL).

second run, 89%; third run, 88%), demonstrating the excellent cycling stability of compound **1**. Additionally, the stability of compound **1** during the reaction was further verified by comparing the FT-IR spectra (Fig. 6(a)) and PXRD patterns (Fig. 6(b)) of the fresh and used catalysts. No significant change was observed after three cycles of reuse. In addition, the XPS spectra of compound **1** after three cycles of reuse were also observed, and the results suggested that the valences of Co and Mo were maintained.

Notably, when the reaction was executed in ambient sunlight for 24 h, **1a** was transformed to **1b** smoothly in 70% yield, which

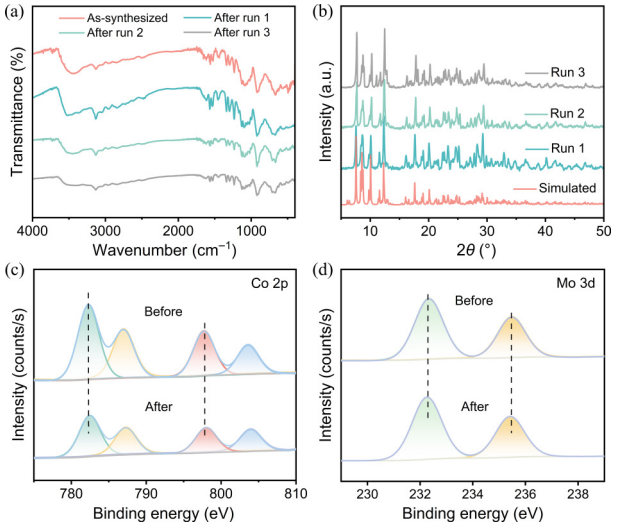

Figure 6 (a) FT-IR spectra of compound **1** before and after catalysis; (b) the PXRD patterns of compound **1** before and after catalysis; the XPS spectra of Co 2p (c) and Mo 3d (d) in compound **1** before and after catalysis.

further demonstrated the utility of the reaction (Fig. 7(a)). At the same time, the 1-mmol-scale synthesis experiment was studied under our reaction conditions, and the target product benzophenone (**1b**) was obtained with a 61% yield (Fig. 7(b)).

We further conducted several control experiments to ascertain the mechanism using 2,6-ditert-butyl-4-methyl phenol and 2,2,6,6-tetramethylpiperidine-1-oxyl as radical scavengers at the optimum conditions, respectively, and a trace product was obtained. Moreover, when benzoquinone was added as the superoxide radical scavenger, the reaction was almost suppressed (Fig. 8(a)). These results suggest that the catalytic reaction proceeded via a radical pathway, with the superoxide radicals serving as essential intermediates. Moreover, electron paramagnetic resonance (EPR) measurements were conducted using 5,5-dimethyl-1-pyrroline N-oxide as a radical trapping agent to detect $O_2^{\bullet-}$ under both dark and light conditions (Fig. 8(b)). The experimental results further confirmed the generation of $O_2^{\bullet-}$ under light irradiation. On–off light experiments for the oxidative cleavage of **1a** to **1b** revealed that the transformation was negligible in the absence of visible-light irradiation (Fig. 8(c)).

A hypothetical mechanism for the oxidative cleavage is proposed based on the aforementioned results. As depicted in Fig. 9, compound **1** can be excited by blue LED light to give the active intermediate **1*** [44], which can oxidize alkenes to furnish an alkene radical cation with the generation of the radical anion **1**. Subsequently, radical anion **1** reduces O_2 to form a superoxide radical anion along with the close of the photocatalytic cycle. Then, the obtained superoxide radical anion can react with the alkene radical cation to give a dioxetane intermediate via [2 + 2]

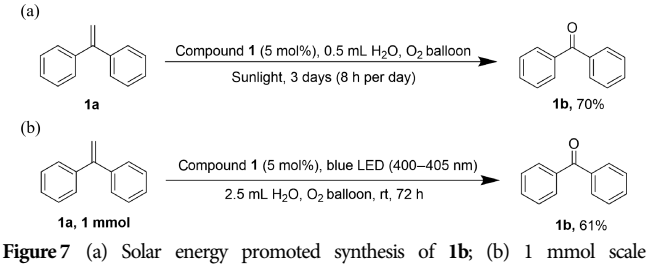

Figure 7 (a) Solar energy promoted synthesis of **1b**; (b) 1 mmol scale experiment.

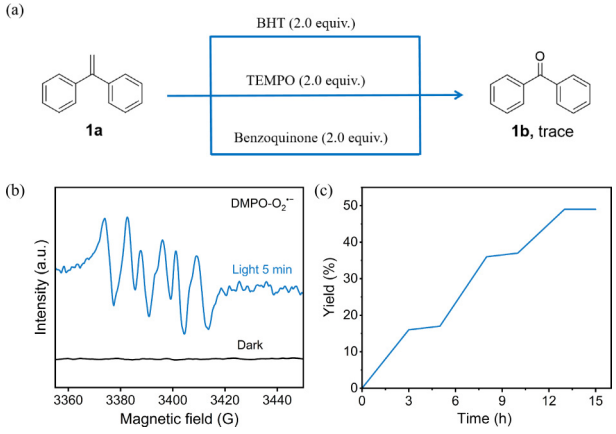

Figure 8 (a) Free radical trapping experiments: **1a** (0.2 mmol), compound **1** (5 mol%), H_2O (0.5 mL), O_2 balloon, 25 °C, blue LED (400–405 nm, 10 W) for 24 h; yields were determined by ^1H NMR calibration using CH_2Br_2 as internal standard; (b) EPR spectra for detecting of superoxide radical: spin trapping of $O_2^{\bullet-}$ with DMPO; (c) on/off light experiments of **1a**.

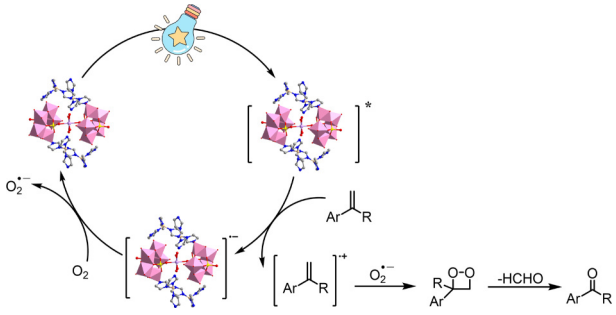

Figure 9 A plausible mechanism for the photocatalytic oxidative cleavage of aromatic alkenes.

cycloaddition [10], which is further transformed into a ketone product by releasing formaldehyde.

4 Conclusions

In summary, a novel boron-imidazolate-based POM catalyst was successfully established for the first time, offering an efficient and convenient heterogeneous photocatalysis strategy to produce value-added carbonyls via the aerobic cleavage of alkenes in aqueous media. The oxidation proceeded under ambient O_2 at room temperature, offering an atom-economical, environmentally benign, and user-friendly method for alkene cleavage. Notably, compound **1** possessed high efficiency and universality in the preparation of carbonyls, enabling the successful preparation of a diverse range of carbonyls with various functional groups. Simultaneously, compound **1** can be readily separated through simple centrifugation and recycled at least three times while retaining its highly efficient catalytic activity. This work offers valuable insights into the conception and fabrication of white-light-responsive POMs as alternative photocatalysts for industrial transformations.

Electronic Supplementary Material: Supplementary material (crystal data, bond distances and angles, hydrogen bonds, bond valence sum calculations, structural figures, FT-IR spectra, PXRD patterns, TGA curves, ^1H NMR, and GC-MS spectra) is available in the online version of this article at https://doi.org/10.26599/POM.2025.9140087.

Data availability

All data needed to support the conclusions in the paper are presented in the manuscript and/or the Electronic Supplementary Material. Additional data related to this paper may be requested from the corresponding author upon request.

Acknowledgements

This work was financially supported by the National Natural Science Foundation of China (No. 21871125) and the Natural Science Foundation of Shandong Province, China (Nos. ZR2023MB018 and ZR2021QB127), the Key Projects of Dongying City School Cooperation Funds (No. SXHZ-2023-02-15), and the foundation of State Key Laboratory of Coal Conversion (No. J24-25-902).

Declaration of competing interest

The authors have no competing interests to declare that are relevant to the content of this article.

Author contribution statement

X. Q. H., J. Y. R., Y. L. Z., Q. L. L. and Q. D. Z: Project administration and writing manuscript. J. J. W. and Z. Y. W.: Experimental design and data collection. G. X. J., H. L. Z. and Y. L.: Data curation. All the authors have approved the final manuscript.

Use of AI statement

During the preparation of this work, the authors used ChatGPT in order to revise the manuscript. After using this tool, the authors reviewed and edited the content as needed and take full responsibility for the content of the publication.

References

[1] Ruffoni, A.; Hampton, C.; Simonetti, M.; Leonori, D. Photoexcited nitroarenes for the oxidative cleavage of alkenes. *Nature* **2022**, *610*, 81–86.

[2] Wise, D. E.; Gogarnoiu, E. S.; Duke, A. D.; Paolillo, J. M.; Vacala, T. L.; Hussain, W. A.; Parasram, M. Photoinduced oxygen transfer using nitroarenes for the anaerobic cleavage of alkenes. *J. Am. Chem. Soc.* **2022**, *144*, 15437–15442.

[3] Li, W. J.; Liu, C. Y.; Liang, L. L.; Zhang, J.; Miao, Y. Q. Visible light-induced aerobic oxidation of an alkene catalyzed by thiobenzoic acid in water. *Org. Chem. Front.* **2024**, *11*, 5429–5436.

[4] Sato, K.; Aoki, M.; Noyori, R. A "green" route to adipic acid: Direct oxidation of cyclohexenes with 30 percent hydrogen peroxide. *Science* **1998**, *281*, 1646–1647.

[5] Schiaffo, C. E.; Dussault, P. H. Ozonolysis in solvent/water mixtures: Direct conversion of alkenes to aldehydes and ketones. *J. Org. Chem.* **2008**, *73*, 4688–4690.

[6] Hart, S. R.; Whitehead, D. C.; Travis, B. R.; Borhan, B. Catalytic oxidative cleavage of olefins promoted by osmium tetroxide and hydrogen peroxide. *Org. Biomol. Chem.* **2011**, *9*, 4741–4744.

[7] Lin, R. Y.; Chen, F.; Jiao, N. Metal-free, NHPI catalyzed oxidative cleavage of C–C double bond using molecular oxygen as oxidant. *Org. Lett.* **2012**, *14*, 4158–4161.

[8] Gonzalez-de-Castro, A.; Xiao, J. L. Green and efficient: Iron-catalyzed selective oxidation of olefins to carbonyls with O_2. *J. Am. Chem. Soc.* **2015**, *137*, 8206–8218.

[9] Huang, Z. L.; Guan, R. P.; Shanmugam, M.; Bennett, E. L.; Robertson, C. M.; Brookfield, A.; McInnes, E. J. L.; Xiao, J. L. Oxidative cleavage of alkenes by O_2 with a non-heme manganese catalyst. *J. Am. Chem. Soc.* **2021**, *143*, 10005–10013.
[10] Xie, P.; Xue, C.; Luo, J. F.; Shi, S. S.; Du, D. D. Decatungstate-mediated solar photooxidative cleavage of C=C bonds using air as an oxidant in water. *Green Chem.* **2021**, *23*, 5936–5943.
[11] Niu, K. K.; Luan, T. X.; Cui, J.; Liu, H.; Xing, L. B.; Li, P. Z. Red-light-based effective photocatalysis of a photosensitive covalent organic framework triggered singlet oxygen. *ACS Catal.* **2024**, *14*, 2631–2641.
[12] Sun, M. L.; Wang, Y. R.; He, W. W.; Zhong, R. L.; Liu, Q. Z.; Xu, S.; Xu, J. M.; Han, X. L.; Ge, X. Y.; Li, S. L. et al. Efficient electron transfer from electron-sponge polyoxometalate to single-metal site metal-organic frameworks for highly selective electroreduction of carbon dioxide. *Small* **2021**, *17*, 2100762.
[13] Cai, A. L.; Hu, G. C.; Chen, W.; Sai, A.; B, Qi.; Song, Y. F. Single-atom Pt anchored polyoxometalate as electron-proton shuttle for efficient photoreduction of CO_2 to CH_4 catalyzed by NiCo layered doubled hydroxide. *Small* **2025**, *21*, 2410343.
[14] Hu, Q. L.; Li, K.; Chen, X. J.; Liu, Y. F.; Yang, G. P. Polyoxometalate catalysts for the synthesis of N-heterocycles. *Polyoxometalates* **2024**, *3*, 9140048.
[15] Gao, Z. Y.; Yang, G. P.; Dong, J.; Liu, P.; Yu, F.; Li, Z.; Zhang, Y. L.; Zhang, M. Y.; Huang, X. Q.; Hu, C. W. Rational fabrication of three imidazole-functionalized ionic-type Pd-polyoxovanadates for aerobic oxidation of 5-hydroxymethulfurfural to 2,5-Diformylfuran. *J. Catal.* **2024**, *429*, 115261.
[16] Dong, C. H.; Liu, X. N.; Li, Z.; Guo, K. H.; Song, C. M.; Zhang, Y. L.; Zhang, M. Y.; Ma, F. F.; Rosei, F.; Zhang, X. X. et al. Boosting electrocatalytic performance of sulfide oxidation on polyoxomolybdates with synergistic effects of CNT-doped aerogel foams. *Adv. Funct. Mater*., in press, DOI: 10.1002/adfm.202418410.
[17] Li, S. J.; Li, N.; Li, G.; Ma, Y. B.; Huang, M. Y.; Xia, Q. C.; Zhao, Q. Y.; Chen, X. N. Silver-modified polyniobotungstate for the visible light-induced simultaneous cleavage of C–C and C–N bonds. *Polyoxometalates* **2023**, *2*, 9140024.
[18] Xia, Z. N.; Wang, L. B.; Zhang, Q.; Li, F. Y.; Xu, L. Fast degradation of phenol over porphyrin-polyoxometalate composite photocatalysts under visible light. *Polyoxometalates* **2022**, *1*, 9140001.
[19] Wang, F.; Jing, C. J.; Ping, J. J.; He, D. Y.; Shang, W. H.; Zeng, M. L.; Wang, N.; Jia, Z. Y. Polyoxometalate-based Cu(II) complexes as the photocatalyst for oxidation of toluene and photodegradation of metronidazole. *Polyoxometalates* **2024**, *3*, 9140067.
[20] Yang, L.; Zhang, Z.; Zhang, C. N.; Wang, X. L. A bifunctional POM-based Cu-viologen complex with mixed octamolybdate clusters for rapid oxidation desulfurization and effective photogeneration of hydrogen. *Rare Met.* **2024**, *43*, 236–246.
[21] Li, S.; Zheng, Y.; Liu, G. C.; Li, X. H.; Zhang, Z.; Wang, X. L. New two fold interpenetrating 3D polyoxovanadate-based metal-organic framework as bifunctional catalyst for the removal of 2-chloroethyl ethyl sulfide and phenolic compounds. *Polyoxometalates* **2024**, *3*, 9140061.
[22] Dong, Y. J.; Su, Z. M.; Guan, W. C(sp^3)-H Trifluoromethylation of pyrrolidine by $[W_{10}O_{32}]^{4-}$/copper synergetic photocatalysis: Theoretical investigation of reactivity and regioselectivity. *Polyoxometalates* **2024**, *3*, 9140068.
[23] Yang, G. P.; Lin, Z. F.; Zhang, X. Z.; Cao, J. W.; Chen, X. J.; Liu, Y. F.; Lin, X. L.; Li, K. Assembly of Y(III)-containing antimonotungstates induced by malic acid with catalytic activity for the synthesis of imidazoles. *Chin. Chem. Lett.* **2024**, *35*, 110274.
[24] Liu, G.; Sun, F. Z.; Fu, S. Q.; Li, Y. J.; Li, Z.; Huang, X. Q. Research progress of polyoxometalates in electrocatalytic chemical conversion. *J. Liaocheng Univ. Nat. Sci. Ed.* **2024**, *37*, 89–102.
[25] Li, S. J.; Ma, Y. B.; Zhao, Y.; Liu, R. J.; Zhao, Y. P.; Dai, X. S.; Ma, N. N.; Streb, C.; Chen, X. N. Hydrogenation catalysis by hydrogen spillover on platinum-functionalized heterogeneous boronic acid-polyoxometalates. *Angew. Chem., Int. Ed.* **2023**, *62*, e202314999.
[26] Yang, G. P.; Liu, Y. F.; Wei, Y. G. Application of polyoxometalates in biomass conversion. *Coord. Chem. Rev.* **2024**, *521*, 216172.
[27] Yang, G. P.; Liu, H. Q.; Zhang, S. H.; Yang, Y. J.; Li, K.; Li, H. L.; Liu, Y. F.; Zang, H. Y. Mixed carboxylate ligands bridging tetra-Pr^{3+}-encapsulated antimonotungstate: Syntheses, structure, and catalytic activity for imidazoles synthesis. *Inorg. Chem.* **2024**, *63*, 22955–22961.
[28] Li, K.; Liu, Y. F.; Yang, G. P.; Zheng, Z. J.; Lin, X. L.; Zhang, Z. B.; Li, S. J.; Liu, Y. H.; Wei, Y. G. Highly-stable silverton-type U^{IV}-containing polyoxomolybdate frameworks for the heterogeneous catalytic synthesis of quinazolinones. *Green Chem.* **2024**, *26*, 6454–6460.
[29] Zhao, H. S.; Zhao, C. Q.; Liu, Z. W.; Yi, J. D.; Liu, X. M.; Ren, J. S.; Qu, X. G. A polyoxometalate-based pathologically activated assay for efficient bioorthogonal catalytic selective therapy. *Angew. Chem., Int. Ed.* **2023**, *135*, e202303989.
[30] Li, K.; Liu, T.; Ying, J.; Tian, A. X.; Wang, X. L. Recent research progress on polyoxometalate-based electrocatalysts in energy generation. *J. Mater. Chem. A* **2024**, *12*, 13576–13604.
[31] Huang, X. Q.; Liu, S.; Liu, G.; Tao, Y. W.; Wang, C. R.; Zhang, Y. L.; Li, Z.; Wang, H. W.; Zhou, Z.; Shen, G. D. et al. An unprecedented 2-fold interpenetrated *lvt* open framework built from Zn_6 ring seamed trivacant polyoxotungstates used for photocatalytic synthesis of pyridine derivatives. *Appl. Catal. B Environ.* **2023**, *323*, 122134.
[32] Gu, J.; Chen, W.; Shan, G. G.; Li, G.; Sun, C.; Wang, X. L.; Su, Z. The roles of polyoxometalates in photocatalytic reduction of carbon dioxide. *Mater. Today Energy* **2021**, *21*, 100760.
[33] Gu, Q. X.; Zhao, X. L.; Meng, M.; Shao, Z. Y.; Zheng, Q.; Xuan, W. M. Crystalline porous ionic salts assembled from polyoxometalates and cationic capsule for the selective photocatalytic aerobic oxidation of aromatic alcohols to aldehydes. *Chin. Chem. Lett.* **2023**, *34*, 107444.
[34] Li, H. J.; Chi, M. Z.; Xin, X.; Wang, R. J.; Liu, T. F.; Lv, H. J.; Yang, G. Y. Highly selective photoreduction of CO_2 catalyzed by the encapsulated heterometallic-substituted polyoxometalate into a photo-responsive metal-organic framework. *Chin. J. Catal.* **2023**, *50*, 343–351.
[35] Li, L.; Yu, Y. T.; Zhang, N. N.; Li, S. H.; Zeng, J. G.; Hua, Y.; Zhang, H. Polyoxometalate (POM)-based crystalline hybrid photochromic materials. *Coord. Chem. Rev.* **2024**, *500*, 215526.
[36] Liu, Y.; Tang, C. S.; Cheng, M.; Chen, M.; Chen, S.; Lei, L.; Chen, Y. S.; Yi, H.; Fu, Y. K.; Li, L. Polyoxometalate@metal-organic framework composites as effective photocatalysts. *ACS Catal.* **2021**, *11*, 13374–13396.
[37] Li, N.; Liu, J.; Dong, B. X.; Lan, Y. Q. Polyoxometalate-based compounds for photo- and electrocatalytic applications. *Angew. Chem., Int. Ed.* **2020**, *59*, 20779–20793.
[38] Chen, X. F.; Wu, H. Z.; Shi, X. J.; Wu, L. X. Polyoxometalate-based frameworks for photocatalysis and photothermal catalysis. *Nanoscale* **2023**, *15*, 9242–9255.
[39] Yu, B.; Zhang, S. M.; Wang, X. Helical microporous nanorods assembled by polyoxometalate clusters for the photocatalytic oxidation of toluene. *Angew. Chem., Int. Ed.* **2021**, *60*, 17404–17409.
[40] Lu, M.; Zhang, M.; Liu, J.; Yu, T. Y.; Chang, J. N.; Shang, L. J.; Li, S. L.; Lan, Y. Q. Confining and highly dispersing single polyoxometalate clusters in covalent organic frameworks by covalent linkages for CO_2 photoreduction. *J. Am. Chem. Soc.* **2022**, *144*, 1861–1871.
[41] Zhang, H. X.; Lu, C.; Zhang, J. Recent applications of multifunctional

boron imidazolate framework materials. *Acc. Mater. Res.* **2023**, *4*, 995–1007.
[42] Hong, Q. L.; Zhang, H. X.; Zhang, J. Synthesis of boron imidazolate frameworks with cobalt clusters for efficient visible-light driven CO_2 reduction. *J. Mater. Chem. A* **2019**, *7*, 17272–17276.
[43] Zhang, H. X.; Hong, Q. L.; Li, J.; Wang, F.; Huang, X. S.; Chen, S. M.; Tu, W. G.; Yu, D. S.; Xu, R.; Zhou, T. H. et al. Isolated square-planar copper center in boron imidazolate nanocages for photocatalytic reduction of CO_2 to CO. *Angew. Chem., Int. Ed.* **2019**, *58*, 11752–11756.
[44] Huang, X. Q.; Liu, S.; Zhou, Z.; Zhang, H. Z.; Gao, Z. Y.; Shen, G. D.; Wang, H. W.; Wang, Z.; Yao, Q. X.; Sun, D. The tail of imidazole regulated the assembly of two robust sandwich-type polyoxotungstate-based open frameworks with efficient visible-white-light-driven catalytic oxidation of sulfides. *Inorg. Chem. Front.* **2023**, *10*, 1465–1474.

Jiajia Wang is a Master's student at the School of Chemistry and Chemical Engineering, Liaocheng University. Her research interests focus on the synthesis of polyoxometalates and their applications in catalytic chemistry.

Yalin Zhang obtained his Ph.D. from Nankai University under the supervision of Prof. Xiaochen Wang in 2020. He is currently a lecturer at the School of Chemistry and Chemical Engineering, Liaocheng University. His research is focused on polyoxometalate-catalyzed organic molecule transformation.

Junyu Ren obtained his Ph.D. in chemistry from University of North Texas under the supervision of Prof. Shengqian Ma in 2022. He currently works as a research fellow at the National University of Singapore. His research is focused on adsorptive separation using framework materials.

Xianqiang Huang is a professor at Liaocheng University. He received his Ph.D. from Beijing Institute of Technology in 2014 under the supervision of Prof. Changwen Hu. He established an independent research group in 2014. His research mainly focuses on are focused on polyoxometalates catalytic chemistry in the field of biomass conversion, organic functional molecule transformation and resource utilization of carbon dioxide conversion.